Backdrivable Miniature Hydrostatic Transmission for Actuation of Anthropomorphic Robot Hands

Hiroshi Kaminaga, Taichi Yamamoto, Junya Ono, and Yoshihiko Nakamura
Department of Mechano-Informatics,
The University of Tokyo,
7-3-1 Hongo, Bunkyo-Ku, Tokyo 113-8656, Japan
Email: kaminaga@ynl.t.u-tokyo.ac.jp

Abstract—**Humanoid robots demand high performance on actuators, such as power-to-weight ratio, durability, occupation volume, and freedom of placement. Also, for robots to interact with unknown objects, flexibility is necessary. Backdrivability is effective when both flexibility and high output torque needs to be realized, which were often contradicting requirement. In this paper, backdrivable hydrostatic transmission is proposed to satisfy requirements above. First, development of hydrostatic actuator including conditions of backdrivability is explained. Second design of backdrivable pump, hydraulic motor and manifold design is explained. Next, design of an anthropomorphic robot hand using developed hydrostatic transmission is discussed. Finally, developed hand is presented and experiments on backdrivability, force sensing, and grasping were performed.**

I. Introduction

Humanoid robots demand high performance on actuators, such as power-to-weight ratio, durability, occupation volume, and freedom of placement. For robots to interact with unknown objects, flexibility is necessary. However, high flexibility and high output torque is often contradicting condition.

Backdrivability is the ability of the mechanical system to move the input axis from the output axis. Most of the commonly used transmissions lack backdrivability. Backdrivability plays large role in actuator flexibility and force controllability. It was not a problem when the system was built for position reference servo, thus in "stiffer the better" manner. However, when the force control is involved, importance of backdrivability became relevant. Without backdrivability, actuators had to realize flexibility by either adding elastic components in series to the actuator output, or by control.

Actuators that have elastic components in series to the transmission are called series elastic actuators (SEA) [1]. It was difficult to have enough flexibility and enough output torque simultaneously. Also effect on servo loop oscillation especially when emulating high stiffness was problem. Impedance control [2] is one of the solutions but since the compliance was emulated by control, they cannot react to quick change in external forces including collisions.

When the backdrivability is realized, compliance of the system is determined by the stiffness of the servo loop. This compliance is passively realized, that makes it possible to react to impulsive inputs. The system can still produce large force when necessary because there is no mechanical limiting factor.

Flexibility of the actuation is especially effective in grasping and manipulation of the objects. Since grasping involves multiple point of contact with uncertainty, robot hands need to deal with uncertain complicated force interaction.

There have been many researches done on mechanism of anthropomorphic robot hands. Salisbury [3] and Jacobsen et al. [4] used metal tendons, and Lovchik and Diftler [5] used linkages and tendons to drive fingers with actuators placed in forearm. Bekey et al. [6] used mechanical linkage to realize more dexterity with less number of actuators. Kawasaki et al. [7], [8], Kaneko et al. [9], and Butterfass et al. [10] developed hand with miniature reducers and miniature motors installed in the hand. Schultz et al. [11], [12] used bellows type pneumatic and water actuators and put all actuator components onto the hand. Nonetheless anthropomorphic robot hand satisfying sufficient dexterity, output torque, and flexibility have not yet developed. One of the large reasons is lack of backdrivability in actuators.

From the point of view of large output, hydraulic actuators have exceptional performance. CB [13] is a humanoid robot using hydraulic actuator and has ability to produce large output force. However, in the hydraulic systems that use servo valves to control hydraulic motors, backdrivability is lost due to the medium isolation at the valve.

Hydrostatic transmission or HST control hydraulic motors by controlling pump rotation and displacement. Because there are no valves used to isolate the medium, system becomes backdrivable when condition on friction is satisfied. HST's controlled by motors are called electrohydrostatic actuators and are used by power-by-wire application of aircrafts [14] due to its large output torque. Bobrow et al. [15] used HST in robot. But for the system that is focused on large output, backdrivability is often not desirable, thus backdrivability of HST is rarely mentioned.

The objectives of this work are the development of novel actuator with backdrivability and application of it to an anthropomorphic robot hand to realize dexterity, high output torque, adaptability, and mechanical durability simultaneously.

In this paper, first, development of backdrivable hydrostatic transmission is explained. Next, developed anthropomorphic hand is presented. Finally, using the developed hand, grasping and backdriving test was performed.

II. Development of Backdrivable Hydrostatic Transmission

A. Backdrivability

The backdrivability problem lies in the apparent asymmetry between the input friction torque and the output friction force of robotic drive mechanisms. Large reduction in the transmission transforms a large displacement of motor rotation into a small displacement of the endeffector. This in turn results in a large endeffector force corresponds to a small motor torque, due to the principle of virtual work.

Static friction inbetween input and output is the source of nonlinear effect of such as neutral zone and hysteresis. For the relationship between the endeffector force and joint torques, it generates an apparent asymmetry that a significantly large force hysteresis at the endeffector corresponds to a rather small torque hysteresis at the motor axis.

The large force hysteresis at the endeffector has an critical importance on the performance of force control not only in mechanics point of view, but also in control stability point of view. Even with high fidelity signal of a force sensor at the wrist near the endeffector, the large force hysteresis in transmission leads to a limited closed loop performance of force control. It is even more critical when contacts are involved in the problem.

We first derive the asymmetry of friction torque of motors and friction force of the end effector by using the coefficient of friction loss which represents in one value the effects of various types of friction, such as static, Coulomb, and viscous frictions.

Consider force transmission in gear drive. Forward transmission torque τ_o^f with input torque τ_i^f is given as follows:

$$\tau_o^f = \frac{r_o}{r_i}\left(1 - \mu_{mech}\cos\alpha\sin\alpha\right)\tau_i^f \tag{1}$$

where α is pressure angle of involute gear, μ_{mech} is friction coefficient, and r_i, r_o are pitch radius of input and output gear respectively. For backdriving, relationship between torque applied to output axis τ_o^b and resulting torque at input axis is:

$$\tau_i^b = \frac{r_i}{r_o}\left(1 - \mu_{mech}\cos\alpha\sin\alpha\right)\tau_o^b \tag{2}$$

For backdriving to be successful, τ_i^b must exceed same value τ_i^{min}, thus:

$$\tau_o^b > \frac{r_o}{r_i}\frac{1}{1 - \mu_{mech}\cos\alpha\sin\alpha}\tau_i^{min} \equiv K\tau_i^{min} \tag{3}$$

Here K is value related to friction loss of torque in the transmission. It can be interpreted that friction hysteresis of input axis is magnified by K when seen from output axis.

For n cascaded gear system, required torque for backdriving becomes as follows.

$$\tau_o^b > \left(\prod_{i=1}^{n} K_i\right)\tau_i^{min} \tag{4}$$

It is easily seen usage of high gear ratio and large number of cascade significantly increases the size of friction hysteresis loop and degrades backdrivability.

B. Miniature Hydrostatic Transmission

To develop an actuator system for humanoid robots, size reduction, power-weight ratio enhancement, and backdrivability improvement are the critical issues.

Hydraulic systems have desirable characteristic that there is only very small mechanical friction in reduction and large reduction ratio can be obtained in single step reduction. However, as mentioned, conventional hydraulic system lacks backdrivability from medium isolation at servo valve. HST does not use servo valves, thus have capability of backdriving with few additional conditions.

For HST to have backdrivability, both pump and hydraulic motor have structure such that when force is applied, it produces pressure, and when pressure is applied, it produces rotation. To have sufficient output torque, adequate reduction ratio is necessary. In hydraulic system, reduction ratio is the ratio of pressure supporting area in pump and hydraulic motor.

Backdrivability ensures the bidirectional force transmission, but to have more control over mechanical property, force control is necessary. Hydraulic system have large advantage over gear driven system that the joint torque can be measured by observing hydraulic pressure with small pressure sensor. Gear drive systems require complicated sensory system to measure joint torque.

Typically, HST is used as CVT from constant engine rotation to variable speed output axis, so variable displacement pump and/or hydraulic motor are commonly used. Variable displacement pumps are often large, complicated and heavy. Variable displacement, however is not necessary in this research because servo motor is used as pump motor, which has advantages over speed controllability.

In this research, trochoid pumps and vane motors are used. Both of them are fixed displacement and have simple structure that enables size reduction. Also, they have structure that is capable of backdriving.

C. Backdrivability Condition

For an actuator to be backdrivable, force applied from output axis of actuator must be greater than force lost in actuator due to static friction. Thus putting torque applied to the output axis τ_o, torque loss in the actuator τ_{loss}, and resulting torque on input axis τi:

$$\tau_i = \tau_o - \tau_{loss} > 0 \tag{5}$$

For HST, assuming friction force in vane motor is small, backdriving condition becomes the condition to turn pump motor axis by applying pressure P.

For trochoid pump, backdriving condition becomes as follows.

$$\tau_i = \left(k_{\tau P}^{pump} - \mu_{mech}\cdot k_{lossP}^{pump}\right)\cdot P - \tau_{seal} > 0 \tag{6}$$

Here, $k_{\tau P}^{pump}$ and k_{lossP}^{pump} are constants determined by pump structure and dimension, μ_{mech} is friction coefficient, and τ_{seal} is friction torque from oil seals that are not related to pressure.

Hence when $\mu_{mech} > k_{\tau P}^{pump}/k_{lossP}^{pump}$, pump cannot rotate regardless of applied pressure, which means backdrivability is never achieved. Thus following is the necessary condition of backdrivability;

$$\mu_{mech} < k_{\tau P}^{pump}/k_{lossP}^{pump} \tag{7}$$

Considering τ_{seal}, (6) is always satisfied with large pressure if (7) is satisfied, so without the limitation of the pressure, (7) is the necessary and sufficient condition of backdrivability.

In typical trochoid pumps, (6) is satisfied roughly with $\mu_{mech} < 0.1$. For hard metal sliding contacts with low viscosity oil, μ_{mech} is ranged from 0.1 to 0.9 [16], which make it practically impossible to achieve backdrivability. On the other hand, for rolling contacts, friction coefficient becomes $\frac{1}{100}$ to $\frac{1}{1000}$ of that of sliding contact [17] that makes the backdrivability highly probable.

D. Modeling of Hydrostatic Transmission

From equations of motion, friction, and flow rate, and motor electronics, they are reduced to followings with parameters listed in Table I:

$$\left(sJ_p + K_{PFFQ}\right)\dot{\theta}_p + \left(K_{PFFP} + K_{PF} + K_{PP}^{-1}\right)P_{out} - N\tau_a = 0 \tag{8}$$

$$\frac{NK_TK_{EMF}}{sL_a+R_a} + \tau_a = \frac{K_T}{sL_a+R_a}v \tag{9}$$

$$\left(sJ_m + K_{MFFQ}\right)\dot{\theta}_m - \left(K_{MT} - K_{MFFP} - K_{MF}\right)P_{out} + \left(K_{MT} - K_{MFFP} - K_{MF}\right)K_\lambda V_t = -d \tag{10}$$

$$\left(K_{MV} + K_{MLQ}\right)\dot{\theta}_m + K_{MLP}P_{out} - \left(1 + K_{MLP}K_\lambda\right)V_t = 0 \tag{11}$$

$$\left(K_{PLQ} - K_{PV}\right)\dot{\theta}_p + K_{PLP}P_{out} + V_t = 0 \tag{12}$$

It should be noted that the equations are linear to the coefficients, coefficients may vary under operating state which makes equations nonlinear in total.

III. Design of Backdrivable Pump

From the analysis in section II-C, it became clear that to realize the backdrivability, all the rotating components should be supported by ball or roller bearings. Since ball bearing have gaps, it was necessary to reserve some gaps between the side of the rotor and pump casing to prevent collision. On the other hand, internal leakage increases by cube of gaps, degrading efficiency significantly. To solve this problem, constant force preloading on bearings were introduced. Fig. 1 shows isometric view of the designed pump. To minimize unnecessary gap, all of the gaps along the axis is adjustable with shims. Bearings supporting pump rotors are preloaded with coil springs to eliminate axial gaps.

Pumps are driven by brushless DC servo motor to achieve high power and high durability. Servo motors are equipped with encoders to detect position and velocity of pumps.

TABLE I
NOMENCLATURE

Name	Description	Unit
$J_{\{p,m\}}$	Moment of inertia load of pump (vane motor)	kgm^2
L_a	Coil inductance of pump motor	H
R_a	Coil Resistance of pump motor	Ω
v	Applied voltage to pump motor	V
K_T	Torque coefficient of pump motor	Nm/A
K_{EMF}	EMF coefficient of pump motor	V/(rad/s)
$\theta_{\{p,m\}}$	Angular position of pump inner rotor (vane motor)	rad
τ_a	Output torque of motor rotor	Nm
P_{out}	Output pressure of pump	Pa
N	Reduction Ratio of pump motor gear head	
d	Disturbance torque of vane motor	Nm
$V_{\{t,p\}}$	Flow rate in the tube (pump)	m^3/s
$K_{\{P,M\}F}$	Mechanical friction in pump (vane motor)	Nm/Pa
$K_{\{P,M\}FFP}$	Viscous friction in pump (vane motor) per pressure	Nm/Pa
$K_{\{P,M\}FFQ}$	Viscous friction in pump (vane motor) per speed	Nm/(rad/s)
$K_{\{P,M\}LP}$	Leak flow regarding pressure in pump (vane motor)	m^3/Pa
$K_{\{P,M\}LQ}$	Leak flow regarding speed in pump (vane motor)	m^3/(rad/s)
$K_{\{P,M\}V}$	Pumping flow regarding speed in pump (vane motor)	m^3/(rad/s)
K_{PP}	Pumping pressure per torque of pump	Pa/Nm
K_{MT}	Rotation torque per pressure of vane motor	Nm/Pa
K_λ	Pressure loss in tubing	$Pa \cdot s/m^3$

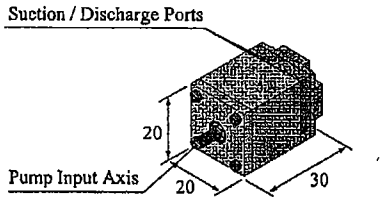

Fig. 1. CAD Model of Miniature Trochoid Pump

IV. The Vane Motor and Manifold Design

The designed actuator consists of mainly three components: main compartment, side seals, and vane with output axis. Fig. 2 depicts the principle of the developed vane motor. Main compartment is made of polycarbonate and consists of two layers to form channel to improve ease of tubing. Two layers of compartment are bonded permanently with adhesives. Side seals are made of aluminum alloy with bearings and oil seals installed. Output shaft on the vane is made with stainless steel and the vane is made of low-friction plastic, Oiles #80 of Oiles Corp. Potentiometer is installed on the output axis to measure link position.

Four types of vane motors with different output torque were developed to be used in the joint of hand with different torque requirements.

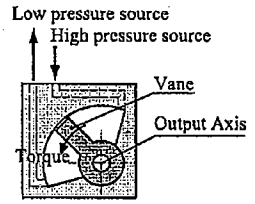

Fig. 2. Structure of the Vane Motor

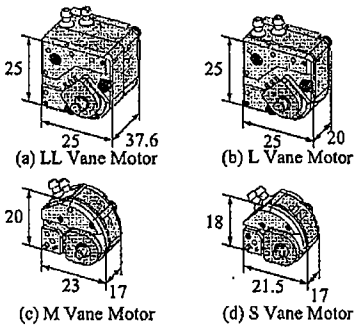

Fig. 3. Developed Vane Motors

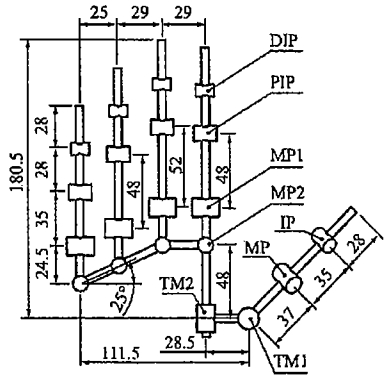

Fig. 4. Joint Assignment and Link Dimension of Developed Anthropomorphic Robot Hand

TABLE II
JOINTS AND ACTUATORS USED IN DEVELOPED HAND

Fingers				
Joint	DIP	PIP	MP1	MP2
Vane Size	S	M	L	M
Thumb				
Joint	IP	MP	TM1	TM2
Vane Size	M	L	LL	L

Forming manifold by lamination was applied also to build pump manifold assembly. Because there is necessity to mount pumps in high density, pumps are mounted in forearm with manifold. Manifolds by lamination technique enabled high density three dimensional tubing without casting. These manifolds are designed to serve as channels as well as structures to reduce number of components to reduce weight.

V. ANTHROPOMORPHIC ROBOT HAND

Motion of the human hand is generated by complicated bone-tendon interaction. It is neither realistic to realize the movements totally by robot hand, nor it is necessary. In this research, to realize maximum DOF's and still maintain robustness, 20 DOF's were selected as shown in Fig. 4 as representative of complicated DOF's.

Hand is equipped with four fingers and a thumb, each with four DOF. Fingers have distal interphalangeal (DIP) joint, proximal interphalangeal (PIP) joint and metacarpal phalangeal (MP) joint. MP joint is realized with flexion/extension joint and adduction/abduction joint. Movement of metacarpal base was omitted to maintain the rigidity of the hand structure. In human, DIP and PIP movements are not totally independent from the interference of the force from tendons. In this hand, DIP and PIP on fingers are connected in parallel. To actuators connected in parallel, same pressure is supplied, thus torque is distributed mechanically. Table II shows the usage of developed actuators shown in Fig. 3, in the hand. Force at the fingertip of pointing finger is estimated approximately 22 (N).

Base joint of the thumb of man is generated by complicated movements of trapeziometacarpal (TM) joint. This movement was simplified with two joints. MP and interphalangeal (IP) joints are actuated independently. In total, there are 20 DOF's, among them, 16 are independent because of four pairs of parallel connections.

Thumb needs to be positioned opposing other fingers in order to realize effective grasping. As a measure, thumb was positioned so it can oppose middle finger.

The developed vane motors are interconnected with linkage to form a finger. MP2 joint axes are equipped with additional bearings to bear large moment load from grasping. Actuator ports are connected with polyurethane tubes. All fingertips are equipped with three axes force sensors to measure operating force. Pressure sensors are installed in all pumps for the torque monitoring.

Fig. 5 shows the developed hand assembled with pump complex. At this present, there is no actuators on wrist, thus large space is reserved for future development.

VI. EXPERIMENTS

A. Backdrivability

To verify backdrivability of the developed system, constant torque was applied to output axis using pulley and weight. Backdriving was verified by observing pump rotation by encoder attached to the pump motor. The test was done with four different loads, each of them five runs. Test result is shown in Table III and pump angle trajectory is shown in Fig. 6.

From this experiment, it is confirmed that the HST backdrives from pressure of around 250(mNm).

The term intermittent mean backdriving was observed in some occasion but not all. One reason of this is due to static

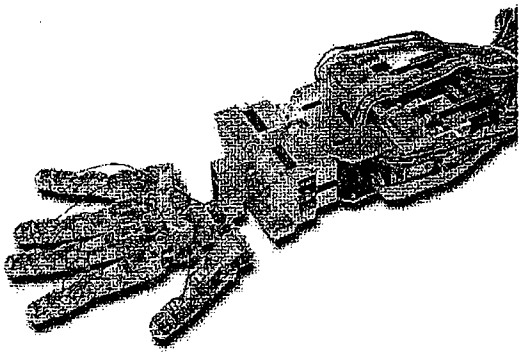

Fig. 5. Assembled Hand and Forearm Pump Complex (Tubes are not shown)

TABLE III
BACKDRIVING TEST RESULT

Applied Torque(mNm)	Backdrive	(success/total)
196	none	(0/5)
245	intermittent	(1/5)
294	intermittent	(3/5)
392	always	(5/5)

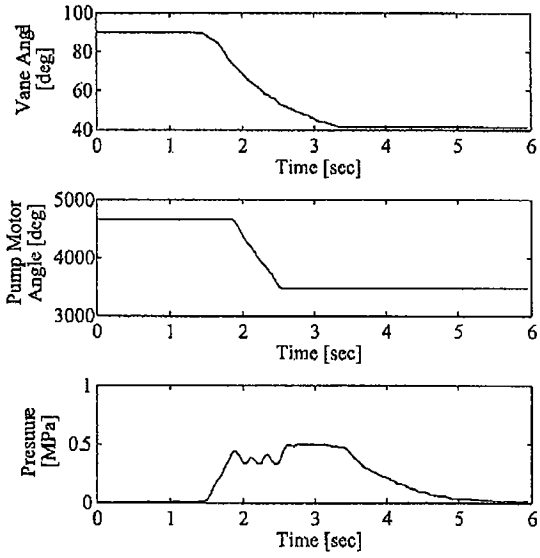

Fig. 6. Backdriving Test with Input Torque to L Size Vane Motor of 392 (mNm)

friction of seals. When all the friction becomes dynamic, then backdriving occurs and if one part sticks, then whole transmission stops backdriving. This is likely to happen in marginal conditions. Another reason is due to machining precision of components. There are some meshing of trochoid gear teeth stiffer than the others. It is hard to backdrive when meshing is in that state. This is also observed in latter half of backdriving in Fig. 6.

B. Torque Sensing by Pressure Measurement

In hydraulic system, force acting on the output axis can be observed by measuring hydraulic oil pressure. In developed HST, pressure and torque relationship is derived from (10) and (11) and written in following from when not accelerating, where $k_{loss\{1,2\}}$ are constants under constant friction condition.

$$d = k_{loss1}P - k_{loss2}\dot{\theta}_m \tag{13}$$

The experiment setup is similar to that of backdriving. Instead of constant load, vane axis was driven by linear stage with load cell to measure the actual load.

Output torque was measured with load cell under different pump motor voltage input and different output axis speed. Experiment result is shown in Fig. 7.

From least-square estimation, it was calculated as follows.

$$\begin{aligned} k_{loss1} &= 4.76 \times 10^{-7}(\mathrm{Nm/Pa}) \\ k_{loss2} &= 0.407(\mathrm{Nms/rad}) \end{aligned}$$

RMS of estimation error was 0.0079[Nm].

C. Grasping

Grasping was performed with the developed hand. It was performed using forefinger and thumb, with proportional control on joint position. Target positions of the joints are intentionally set to values that collide with grasping objects to see the behavior of grasping with effect of flexibility and backdrivability. Thin and thick drink PET bottles were chosen as grasping objects.

Fig. 8 shows the snapshot of grasping test of thick bottle. Fig. 9 shows selected joint angle trajectory.

Grasping was stable in all cases, where if it lacked backdrivability, transmission may cause failure due to over load. Since joints on forefinger are smaller than the one mounted on thumb, they do not reach target angle. Especially, PIP of forefinger was backdriven by the grasping force from thumb.

VII. CONCLUSIONS

In this paper, backdrivable hydrostatic actuators for humanoid robots were developed. First, importance, and condition of backdrivability is discussed. Analysis of backdrivability was performed. To form hydrostatic transmission, trochoid pumps and vane motors are used. Backdrivable trochoid pump and four types of vane motors with different displacement were developed. Using the developed actuators, an anthropomorphic robot hand with 20 degree of freedom was developed. Finally, backdriving, force sensing, and grasping were performed. The result of backdrivability test showed minimum backdriving pressure of about 250 (mNm) for L vane motor. Result of force sensing test showed the fitting error of data to the model equation of 0.79×10^{-3}(Nm), which is under 2% of the

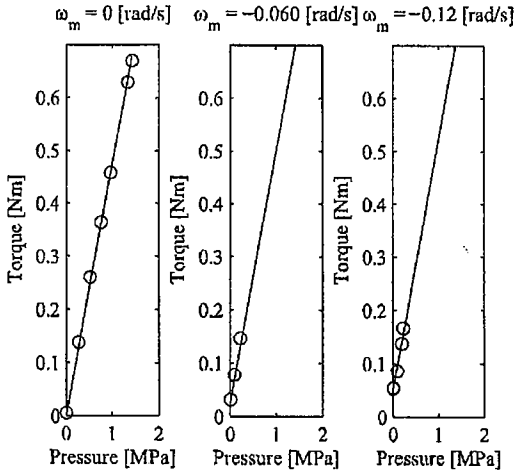

Fig. 7. Torque Sensing Data. Circular markers are experiment data. The line is least-square fitting.

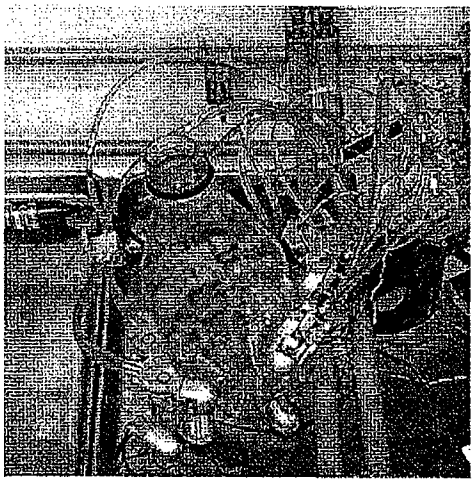

Fig. 8. Grasp Operation with Thick Object

range of torque to be used. Grasping test showed durability, flexibility and backdrivability of the hand.

ACKNOWLEDGEMENTS

This work was supported by "IRT Foundation to Support Man and Aging Society" under Special Coordination Funds for Promoting Science and Technology from MEXT.

REFERENCES

[1] G. A. Pratt and M. M. Williamson, "Series Elastic Actuators," in *Proc. of IEE/RSJ Int'l Conf. on Intelligent Robots and Systems*, vol. 1, 1995, pp. 399–406.

[2] N. Hogan, "Impedance Control: An Approach to Manipulation: Part I - Theory," *Trans. of ASME J. Dyn. Sys. Meas. Ctrl*, vol. 1, no. 107, pp. 1–7, 1985.

[3] J. K. Salisbury, "Design and control of an articulated hand," in *Proc. of the 1st Int'l Symposium on Design and Synthesis*, 1984.

[4] S. C. Jacobsen, E. K. Iversen, D. F. Knutti, R. T. Johnson, and K. B. Biggers, "Design of the Utah/M.I.T. dextrous hand," in *Proc. of IEEE Int'l Conf. on Robotics and Automation*, 1986, pp. 1520–1532.

[5] C. S. Lovchik and M. A. Diftler, "The Robonaut Hand: A Desterous Robot Hand for Space," in *Proc. of IEEE Int'l Conf. on Robotics and Automation*, 1999, pp. 907–912.

[6] G. A. Bekey, R. Tomovic, and I. Zeljkovic, "Control architecture for the Belgrade/USC hand," in *Dextrous Robot Hands*. Springer-Verlag, 1990.

[7] H. Kawasaki, T. Komatsu, and K. Uchiyama, "Dexterous anthropomorphic robot hand with distributed tactile sensor: Gifu hand ii," in *IEEE/ASME Trans. on Mechatronics*, 2002, pp. 296–303.

[8] T. Mouri, H. Kawasaki, K. Umebayashi, Y. Nishimoto, H. Shimoura, and Y. Ishigure, "Development of robot hand for education/training of rehabilitation," in *Proc. of 24th Annual Conf. of the Robotics Society of Japan*, vol. CD-ROM, 2006, p. 2I25, in Japanese.

[9] K. Kaneko, K. Harada, and F. Kanehiro, "Outline of life-size multi-fingered hand that is in progress," in *Proc. of 24th Annual Conf. of the Robotics Society of Japan*, vol. CD-ROM, 2006, p. 2H17, in Japanese.

[10] J. Butterfass, M. Grebenstein, H. Liu, and G. Hirzinger, "DLR-hand II: Next generation of a dextrous robot hand," in *Proc. of IEEE Int'l Conf. on Robotics and Automation*, 2001, pp. 109–114.

[11] S. Schulz, C. Pylatiuk, and G. Bretthauer, "A new ultralight anthropomorphic hand," in *Proc. of IEEE Int'l Conf. on Robotics and Automation*, 2001, pp. 1–6.

[12] A. Kargov, T. Asfour, C. Pylatiuk, R. Oberle, H. Klosek, S. Schulz, K. Regenstein, G. Bretthauer, and R. Dillmann, "Development of an Anthropomorphic Hand for a Mobile Assistive Robot," in *Proc. of Int'l Conf. on Rehabilitation Robotics*, 2005, pp. 182–186.

[13] G. Cheng, S. H. Hyon, J. Morimoto, A. Ude, G. Colvin, W. Scroggin, and S. C. Jacobsen, "CB: A Humanoid Research Platform for Exploring NeuroScience," in *Proc. of 6th IEEE-RAS Int'l Conf. on Humanoid Robots*, 2006, pp. 182–187.

[14] R. Navarro, "Performance of an Electro-Hydrostatic Actuator on the F-18 Systems Research Aircraft," NASA," Technical Memorandum, 1997.

[15] J. E. Bobrow and J. Desai, "Modeling and Analysis of a High-Torque, Hydrostatic Actuator for Robotic Applications," *Experimental Robotics*, pp. 215–228, 1989.

[16] B. Bhushan and B. K. Gupta, *Handbook of Tribology*. McGraw-Hill, 1991.

[17] E. R. Booser, *Tribology Data Handbook*. CRC Press, 1997.

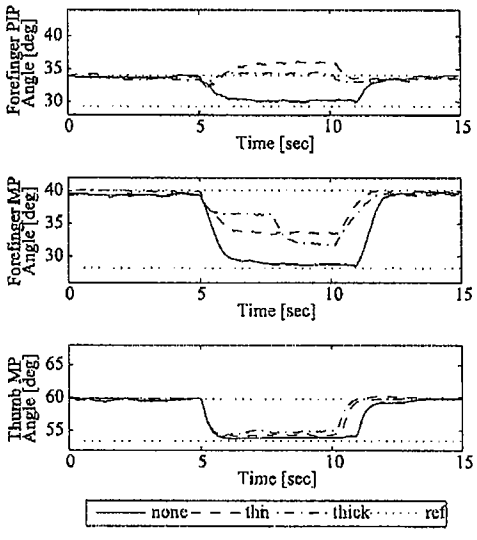

Fig. 9. Joint Trajectory of Grasping Operation